Deep-Sea Research II 131 (2016) 111–122

Contents lists available at ScienceDirect

Deep-Sea Research II

journal homepage: www.elsevier.com/locate/dsr2

Iron biogeochemistry in Antarctic pack ice during SIPEX-2

Delphine Lannuzel [a,b,*], Fanny Chever [c], Pier C. van der Merwe [b], Julie Janssens [a], Arnout Roukaerts [d], Anne-Julie Cavagna [d], Ashley T. Townsend [e], Andrew R. Bowie [a,b], Klaus M. Meiners [b,f]

[a] Institute for Marine and Antarctic Studies, University of Tasmania, Locked Bag 129, Hobart, TAS 7001, Australia
[b] Antarctic Climate and Ecosystems CRC, University of Tasmania, Private Bag 80, Hobart, TAS 7001, Australia
[c] Ocean and Earth Science, National Oceanography Centre Southampton, University of Southampton, Southampton SO14 3ZH, United Kingdom
[d] Analytical, Environmental & Geo-Chemistry, Vrije Universiteit, Brussel, Pleinlaan 2, B-1050 Brussels, Belgium
[e] Central Science Laboratory, University of Tasmania, Private Bag 74, Hobart, TAS 7001, Australia
[f] Australian Antarctic Division, 203 Channel Highway, Kingston, TAS 7050, Australia

ARTICLE INFO

Available online 11 December 2014

Keywords:
Sea ice
Iron
Antarctica
Southern Ocean
Primary production

ABSTRACT

Our study quantified the spatial and temporal distribution of Fe and ancillary biogeochemical parameters at six stations visited during an interdisciplinary Australian Antarctic marine science voyage (SIPEX-2) within the East Antarctic first-year pack ice zone during September–October 2012. Unlike previous studies in the area, the sea ice Chlorophyll *a*, Particulate Organic Carbon and Nitrogen (POC and PON) maxima did not occur at the ice/water interface because of the snow loading and dynamic processes under which the sea ice formed. Iron in sea ice ranged from 0.9 to 17.4 nM for the dissolved (<0.2 μm) fraction and 0.04 to 990 nM for the particulate (>0.2 μm) fraction. Our results highlight that the concentration of particulate Fe in sea ice was highest when approaching the continent. The high POC concentration and high particulate iron to aluminium ratio in sea ice samples demonstrate that 71% of the particulate Fe was biogenic in composition. Our estimated Fe flux from melting pack ice to East Antarctic surface waters over a 30 day melting period was 0.2 μmol/m^2/d of DFe, 2.7 μmol/m^2/d of biogenic PFe and 1.3 μmol/m^2/d of lithogenic PFe. These estimates suggest that the fertilization potential of the particulate fraction of Fe may have been previously underestimated due to the assumption that it is primarily lithogenic in composition. Our new measurements and calculated fluxes indicate that a large fraction of the total Fe pool within sea ice may be bioavailable and therefore, effective in promoting primary productivity in the marginal ice zone.

© 2014 The Authors. Published by Elsevier Ltd. This is an open access article under the CC BY-NC-ND license (http://creativecommons.org/licenses/by-nc-nd/3.0/).

1. Introduction

Marine phytoplankton fix aqueous carbon dioxide (CO_2) within the surface ocean through photosynthesis. This process increases the flux of CO_2 from the atmosphere into the ocean and therefore plays a key role in mitigating green house gas induced global warming (Sarmiento and Gruber, 2006). When light levels are sufficient, phytoplankton growth is limited by the availability of micro-nutrients such as iron (Fe) in remote regions like the Southern Ocean, where external inputs of Fe are low (Martin and Fitzwater, 1988; de Baar et al., 1990). Both laboratory and short-term artificial Fe fertilization experiments unequivocally showed the importance of Fe in controlling phytoplankton production and therefore Fe was one of the factors controlling carbon export into the ocean interior (Boyd et al., 2007). A drawback of artificial fertilization experiments is the difficulty of effectively quantifying carbon export into the ocean interior and estimates vary by 2 orders of magnitude (Blain et al., 2007; Pollard et al., 2009). Although variability in the estimates is high, the CROZEX study in the Southern Ocean showed that the efficiency of natural fertilization from the sub-Antarctic Crozet island was up to 20 times greater than that of an artificially Fe-enriched site (SERIES, Boyd et al., 2004) (Blain et al., 2007; Pollard et al., 2009).

Within Fe limited high nutrient—low chlorophyll waters, multiple naturally Fe-fertilized sites have been identified, including seasonal sea ice, which acts as a 'capacitor' to seasonally store Fe. Antarctic sea ice contains 1–2 orders of magnitude more Fe, organic matter, and chlorophyll *a* than under-ice seawater (Grotti et al., 2005; Lannuzel et al., 2007, 2008; van der Merwe et al., 2009, 2011a,b; de Jong et al., 2013) and triggers ice-edge phytoplankton blooms during the release of these constituents in austral spring (Sedwick et al., 1997; Lancelot et al., 2009). Given that sea-ice formation and retreat affects approximately 40% of the entire Southern Ocean area (Southern Ocean extent $=35\times10^6$ km^2;

* Corresponding author.
E-mail address: delphine.lannuzel@utas.edu.au (D. Lannuzel).

http://dx.doi.org/10.1016/j.dsr2.2014.12.003
0967-0645/© 2014 The Authors. Published by Elsevier Ltd. This is an open access article under the CC BY-NC-ND license (http://creativecommons.org/licenses/by-nc-nd/3.0/).

maximum-minimum Antarctic sea ice extent = 15.2×10^6 km^2; Thomas and Dieckmann, 2003), the "frozen ocean" may therefore constitute the dominant source of Fe to polar waters during annual melting, and therefore plays a key role in drawing down atmospheric CO_2 levels in the climatically-important Southern Ocean. There is an urgent need to evaluate how modern-day climate change will affect the Antarctic sea-ice ecosystem. A pre-requisite for this is to describe and understand present-day sea-ice biogeochemical processes. In this context, new field measurements and sample collection approaches for characterization of sea-ice ecosystem dynamics should be a priority.

The East Antarctic is an ideal location to study the role of sea ice as an ocean fertilizer during the melting season because three consecutive field studies have been specifically dedicated to Fe biogeochemistry in this sector: ARISE in pack ice in 2003 (Sept/Oct, 63.5–65°S/109–117°E; Lannuzel et al., 2007), SIPEX-1 in pack ice in 2007 (Sept/Oct, 64–65.5°S/114–128°E; van der Merwe et al., 2009; 2011a) and a time series in fast ice in 2009 (Casey, Nov, 66°S/110°E; van der Merwe et al., 2011b; Lannuzel et al., 2014). The main outcomes from these studies were that (1) dissolved Fe concentrations vary seasonally rather than spatially (Lannuzel et al., 2010), (2) particulate Fe vary spatially, with higher concentrations observed near the continent or when higher biomass is present (van der Merwe et al., 2011a) and (3) dissolved Fe is released before particulate Fe during spring melt (van der Merwe et al., 2011a). Our previous work also suggested that during the melting season, dissolved Fe released from sea ice could account for 15 to 70% of the primary productivity in the East Antarctic sector, and that the additional Fe supplied in the form of particles may extend the longevity of the ice-edge bloom (Lannuzel et al., 2014). Building on our knowledge of Fe sea-ice biogeochemistry in the area, the major goal of this new field study was 3-staged. First, we wanted to determine if the mode of ice growth (i.e. thermodynamic versus dynamic growth) controls the concentration of dissolved and particulate Fe. The particulate Fe concentration in sea ice was highly variable during three previous field studies in East Antarctica. Therefore, our 2nd aim was to evaluate whether the previously observed variability in pack ice particulate Fe concentration could be explained by its biogenic or lithogenic composition and furthermore, can this differentiation of particulate Fe determine its availability for sea-ice algae and phytoplankton when released into seawater? Finally, based on measured rates of primary productivity in sea ice and ancillary parameters, our last aim was to assess whether macronutrients, Fe or light controlled the local productivity at this time of year.

2. Material and methods

2.1. Collection and handling of samples

Samples were collected during the Australian-led Sea Ice Physics and Ecosystem eXperiment-2 (SIPEX-2) marine science voyage in austral winter/spring 2012 (26 Sept–10 Nov, 64–65°S/116–121°E, Fig. 1). The acid-cleaning protocols for sample bottles and equipment followed the guidelines of GEOTRACES (www.geotraces.org). Contamination-free ice coring equipment developed by Lannuzel et al. (2006) was used to collect ice cores. Ice cores were triple bagged and stored at −18 °C until further processing in the home laboratory. Ice cores were then sectioned under a class-100 laminar flow hood (AirClean 600 PCR workstation, AirClean System) using a medical grade stainless steel bonesaw (Richards Medical), thouroughly rinsed with ultra-high purity water (18.2 MΩ), and ice sections were then allowed to melt at ambient temperature in acid-cleaned 3 L Polyethylene (PE) containers. Melted sea-ice sections were then homogenized by a gentle shake and filtered through 0.2 μm pore size polycarbonate filters (Sterlitech, 47 mm diameter) using Teflon® perfluoroalkoxy (PFA) filtration devices (Savillex, USA) connected to a vacuum pump set on < 2 bar to obtain the particulate (> 0.2 μm) and dissolved (< 0.2 μm) metal fractions. The collected filtrates (< 0.2 μm) were acidified to pH 1.8 using Seastar Baseline® HCl (Choice Analytical) and stored at ambient temperature until analysis in the home laboratory. The filters retaining the particulate material were stored frozen in acid-clean petri dishes until further processing.

Standard physico-chemical and biological parameters such as sea-ice and snow thicknesses, in situ ice temperature, sea-ice and brine salinities, ice texture, chlorophyll *a* (Chl*a*), macro-nutrients (nitrate + nitrite (NO_x), phosphate (PO_4^{3-}), silicic acid ($Si(OH)_4^-$) and ammonium (NH_4^+)), dissolved organic carbon (DOC), and particulate organic carbon and nitrogen (POC and PON) were also determined in each sample, following the methods described in van der Merwe et al. (2009). Theoretical brine volume fractions (V_b/V) were calculated using in situ ice temperatures and bulk ice salinities and relationships from Cox and Weeks (1983). The full ice core length was examined under crossed-polarized light to identify the texture (i.e. columnar vs. granular) according to the method of Langway (1958). Preparation of the thin sections took place in a container kept at −25 °C. The thin sections were obtained by cutting vertical sections of about 6 mm thick using a band saw. Ice sections were then thinned down using a microtome blade to reach a final thickness of 3–4 mm and observed under cross-polarized lights (Fig. 2).

2.2. Analysis of dissolved iron

The acidified filtrates were diluted 5 times, using 2% v-v ultrapure HNO_3 (Seastar Baseline, Choice Analytical) and Fe concentrations were determined directly using sector field inductively coupled plasma magnetic sector mass spectrometry (SF-ICP-MS; Element 2) following the method described in Lannuzel et al. (2014). Results for procedural blanks and limits of detection are presented in Table 1.

2.3. Analysis of particulate iron and aluminium

Filters retaining particulate material (> 0.2 μm) were digested in a mixture of strong, ultrapure acids (750 μL 12 N HCl, 250 μL 40% HF, 250 μL 14 N HNO_3) in 15 mL Teflon® perfluoroalkoxy (PFA) (Savillex, USA) on a Teflon coated graphite digestion hot plate housed in a bench-top fume hood (all *Digi*PREP from SCP Science, France) coupled with HEPA® filters to ensure clean air input at 95 °C for 12 h, then dry evaporated for 4 h and re-suspended in 2% v-v HNO_3 (Seastar Baseline, Choice Analytical). The procedure was applied to filter blanks and certified reference materials BCR-414 and MESS-3 to verify the recovery of the acid digestion treatment. The concentrations of particulate metals were then determined by SF–ICP–MS (Bowie et al., 2010). Results for procedural blanks, limits of detection and certified reference materials are presented in Tables 1 and 2 and were found fit for purpose. Although we obtained the concentrations of 18 elements in our sea-ice samples, we only dicuss Fe here, and used aluminium (Al) concentrations to fingerprint Fe sources. The other elements will be reported and discussed in a companion paper.

For statistical analysis, we used a Spearman's Rho correlation because the data was non-normally distributed (i.e. non-parametric), with Spearman's rho correlation coefficient R, the number of data points n, and the level of significance $p < 0.01$ or $p < 0.05$ (Table 3).

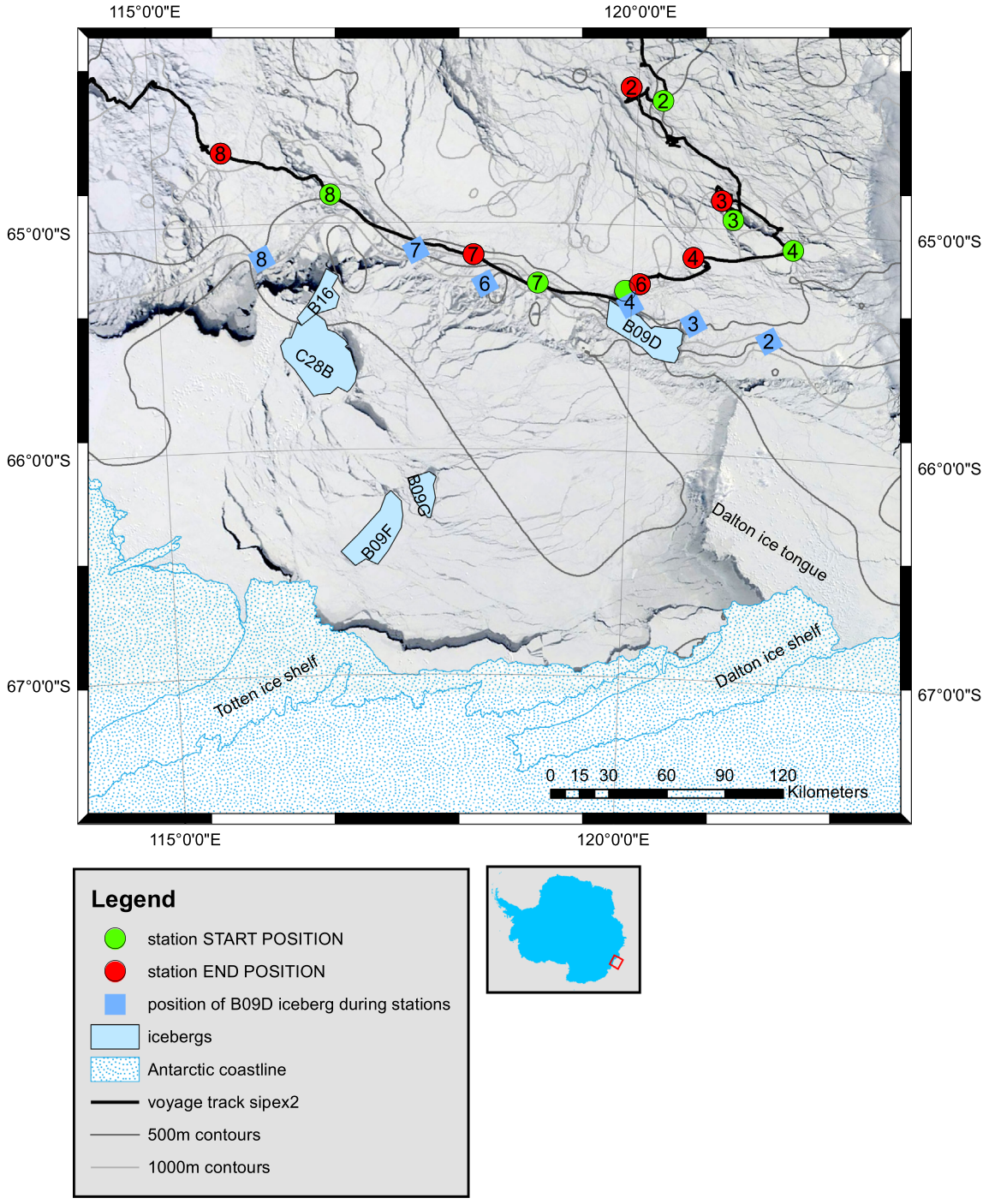

Fig. 1. Bathymetry, sea-ice cover, ship track and locations of the ice stations visited during the SIPEX-2 voyage. Due to the westward drift of pack ice, the start and end positions of each station are indicated on the map. Station 2 was sampled on 26.11.2012, station 3 on 03.10.2012, station 4 on 07.10.2012, station 6 on 13.10.2012, station 7 on 19.10.2012 and station 8 on 29.10.2012. Note the location of iceberg B09D during each ice station. The projection is South Pole Stereographic and the map has been rotated 118° CCW. All data was provided by the Australian Antarctic Data Centre (https://data.aad.gov.au/). Bathymetry data supplied by IBCSO project Arndt et al. (no date). Coastal polygon supplied by SCAR, Antarctic Digital Database is copyright © 1993–2014 Scientific Committee on Antarctic Research. MODIS images downloaded from NASA Worldview (https://earthdata.nasa.gov/labs/worldview/).

3. Results

3.1. Sea-ice physical properties

Apart from station 2 which had a thin cover of 0.05 m of snow, the rest of the sites were covered with a very thick layer of snow, ranging from 0.25 m at station 3 to 0.74 m at station 6 (Fig. 2, average 0.39 m). The sea-ice cores collected on our sites ranged from 0.72 to 1.43 m in thickness (average 0.93 m). Texture-wise, station 3 was the only typical first-year pack-ice station, with 0.02 m of granular ice underlain by columnar ice. Station 4 also showed some first year sea-ice features, with 0.29 m of granular ice underlain by 0.61 m of columnar ice. Overall, granular ice however dominated the overall ice textures at 64% (Fig. 2). The snow thickness represented on average 30% of the total ice thickness. Station 6 showed evidence of rafting processes with the superposition of granular ice on top of columnar ice in three consecutive layers.

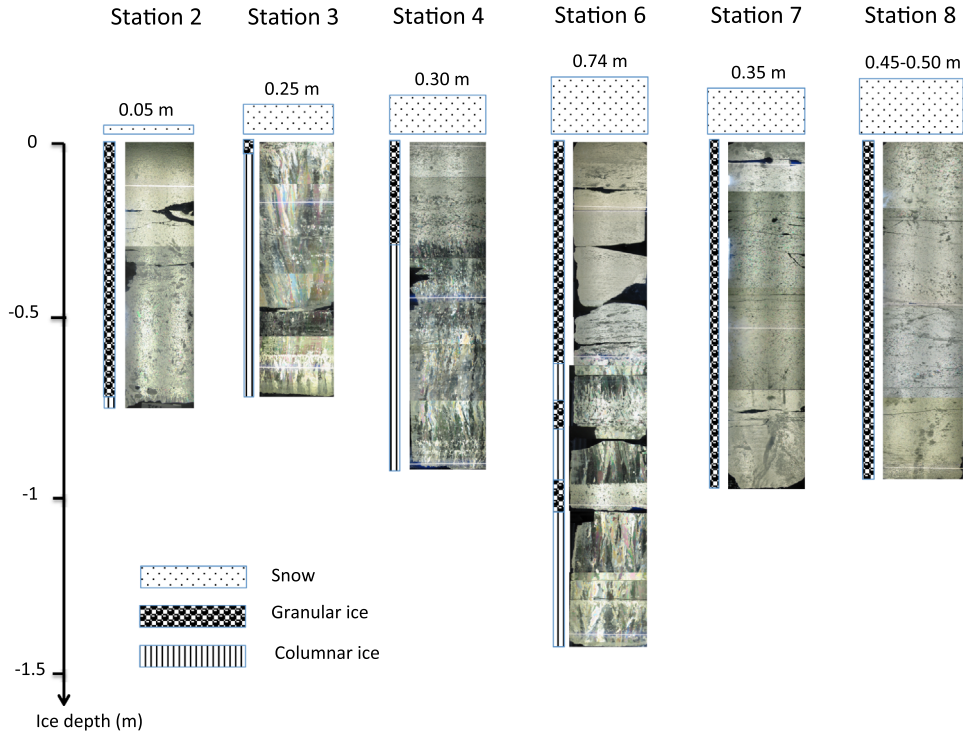

Fig. 2. Snow thickness (in m), ice thickness (in m) and sea-ice textures (granular and columnar) obtained from thin sections observed under polarized light.

Table 1
ICP–SFMS results in μg/L for procedural digest filter and rinse solution blanks. The limit of detection (LOD) is 3 times the standard deviation of the filter blank.

	Fe (μg/L)	Al (μg/L)
0.2 μm PC filter		
Average filter blank ($n=3$)	0.99 ± 0.25	1.38 ± 0.61
LOD	0.750	1.82
2% HNO_3		
Average blank ($n=10$)	0.04 ± 0.01	0.06 ± 0.03
LOD	0.03	0.09

Table 2
ICP-SFMS results in mg/kg for certified referenced material ($n=8$), [indicative value].

	Fe (mg/kg)	Al (mg/kg)
BCR-414		
[Indicative]	$[1850 \pm 190]$	$[1800 \pm 30]$
Measured	1880 ± 60	2639 ± 80
MESS-3		
Certified	43400 ± 1100	85900 ± 2300
Measured	39076 ± 1533	76439 ± 3321

The mean in situ sea-ice temperatures increased from −4.8 °C at station 3, to −3.0 °C at station 4 and up to −1.8 °C at the remaining sites. The ice temperature profiles were nearly isothermal for stations 2, 6, 7 and 8 (Fig. 3A), probably because of the thick snow cover pushing the ice deep into the ocean and insulating it against the atmosphere. The mean air temperature increased from −22.8 °C at station 3, to −10.7 °C at station 4 and up to −2.9 °C at station 6 (Fig. 3A).

Sea-ice salinities ranged from 3.9 to 18.5, and the vertical profiles were highly heterogeneous overall. Salinities were generally higher in the surface layers. Station 3 had the only "C-shaped" salinity profile of the voyage (Fig. 3B), which is typically observed in first year winter pack ice (van der Merwe et al., 2009).

The brine volume ratio V_b/V (where V_b=brine volume and V=volume of bulk sea ice) can be used as an indicator of sea ice permeability. Typically, in columnar ice, when $V_b/V < 5\%$ (for salinity of 5 and ice temperature of −5 °C), the ice is considered impermeable (Golden et al., 1998). Saenz and Arrigo (2012) have suggested that the permeability threshold of granular ice, formed by frazil ice accumulation or due to snow ice formation, may be higher than the permeability threshold of columnar ice, formed by congelation growth. This can be explained by a more random distribution of brine pockets and channels in granular sea ice. In our samples, granular ice dominated, and the mean brine volume ratio (V_b/V) was 8.3% on average at station 3, 12.0% at station 4 and 14.5–19.6% at the warmer sites. Significant correlations (non-parametric, Spearman's rho=0.56, $n=35$, $p<0.01$) were observed between brine volume and ice temperature. Therefore the increase in average brine volume appeared to be driven by an increase in average ice temperature, which is ultimately controlled by increasing ambient air temperatures (Fig. 3A). Station 3 had intermediate ice sections below the critical V_b/V of 5% for columnar ice, indicating the impermeable nature of these sections within the ice. All the other stations had $V_b/V > 10\%$, suggesting sea-ice melting was already underway at the time of sampling (Fig. 3C).

3.2. Sea-ice biogeochemistry

3.2.1. Macro-nutrients, Chla, DOC, POC and PON

Sea-ice concentration ranges of NO_x, $Si(OH)_4^-$, PO_4^{3-} and NH_4^+ were 0.1–8.2 μM, 1.7–26.6 μM, 0.1–1.9 μM and 0.1–14.3 μM, respectively (Fig. 4A–D). Macro-nutrient concentrations are also shown plotted versus sea-ice salinity (Fig. 4E–H). The theoretical dilution line (TDL) was plotted by using the salinity and macro-nutrients concentration in seawater collected at 1 m below the sea ice. Silicic acid behaved conservatively with salinity, although most of the data points were slightly above the TDL (Fig. 4F). The relationship between $Si(OH)_4^-$ and ice salinity was statistically significant (Table 3), however, all other macro-nutrients deviated from their respective TDL. NO_x concentrations were significantly reduced

Table 3
Spearman's rank correlation coefficients in sea ice. The number of samples (n) is the sum of all sections and sites used in the correlation analysis. The bold shading marks the significant correlations. Sigma 2-tailed with *=$p<0.05$; **=$p<0.01$.

		V_b/V	Chl*a*	POC	PON	DOC	NH_4^+	NO_x	PO_4^{3-}	$Si(OH)_4^-$	DFe	PFe
Salinity	Correlation	**0.377***	−0.010	0.000	0.158	0.202	0.259	0.261	0.318	**0.737****	0.130	0.099
	Sigma	0.023	0.952	0.999	0.358	0.238	0.127	0.136	0.059	0.000	0.448	0.568
	n	36	36	36	36	36	36	34	36	34	36	36
V_b/V	Correlation		−0.087	0.043	0.195	0.172	0.154	**0.722****	**0.347***	**0.520****	**0.549****	0.314
	Sigma		0.615	0.802	0.254	0.317	0.369	0.000	0.038	0.002	0.001	0.062
	n		36	36	36	36	36	34	36	34	36	36
Chl*a*	Correlation			**0.557****	**0.600****	0.185	**0.436****	0.048	**0.516****	−0.076	−0.056	0.251
	Sigma			0.000	0.000	0.280	0.008	0.789	0.001	0.669	0.746	0.139
	n			36	36	36	36	34	36	34	36	36
POC	Correlation				**0.891****	**0.666****	**0.684****	−0.113	**0.561****	0.049	0.022	**0.397***
	Sigma				0.000	0.000	0.000	0.525	0.000	0.784	0.898	0.016
	n				36	36	36	34	36	34	36	36
PON	Correlation					**0.514****	**0.736****	0.134	**0.770****	0.193	0.053	**0.376***
	Sigma					0.001	0.000	0.451	0.000	0.275	0.760	0.024
	n					36	36	34	36	34	36	36
DOC	Correlation						**0.386***	−0.141	0.250	0.119	0.113	**0.416***
	Sigma						0.020	0.426	0.141	0.503	0.513	0.012
	n						36	34	36	34	36	36
NH_4^+	Correlation							0.076	**0.531****	0.308	0.085	**0.428****
	Sigma							0.671	0.001	0.077	0.622	0.009
	n							34	36	34	36	36
NO_x	Correlation								**0.485****	**0.525****	0.323	**0.348***
	Sigma								0.004	0.002	0.063	0.044
	n								34	33	34	34
PO_4^{3-} –	Correlation									**0.478****	0.125	0.296
	Sigma									0.004	0.467	0.080
	n									34	36	36
$Si(OH)_4^-$	Correlation										**0.371***	0.245
	Sigma										0.031	0.163
	n										34	34
DFe	Correlation											**0.575****
	Sigma											0.000
	n											36

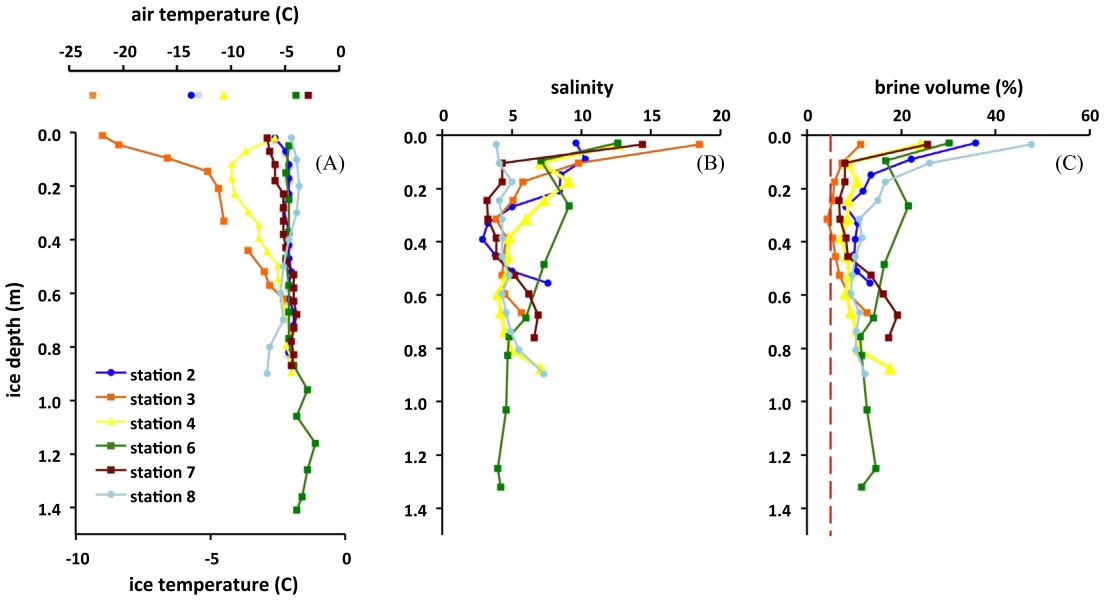

Fig. 3. (A) Air and sea-ice temperatures, (B) salinity and (C) brine volume ratios (%) during SIPEX-2. The red dashed line marks the 5% brine volume permeability threshold for columnar ice. (For interpretation of the references to color in this figure legend, the reader is referred to the web version of this article.)

relative to the TDL (Fig. 4E), indicating a drawdown of NO_x in sea ice, sometimes until complete exhaustion (station 7). Conversely, PO_4^{3-} deviated above and below the TDL while NH_4^+ concentrations were generally below the TDL (Fig. 4G and H), indicating accumulation of NH_4^+.

The Chl*a* concentration in sea ice ranged from <0.02 μg/L at station 6 to 13.7 μg/L at station 7, with an overall average Chl*a* concentration of 2.2 ± 2.5 μg/L (Fig. 5A). The highest Chl*a* concentrations occurred in sea-ice interior layers, except for station 6 where Chl*a* maximum was in the bottom ice layer.

Dissolved organic carbon in sea ice ranged from 0.15 and 2.66 mg/L (average 1.4 ± 0.7 mg/L). Stations 4 and 7 respectively exhibited the lowest and highest DOC values. Similar to Chl*a*, the DOC maxima did not occur at the ice/water interface (Fig. 5B).

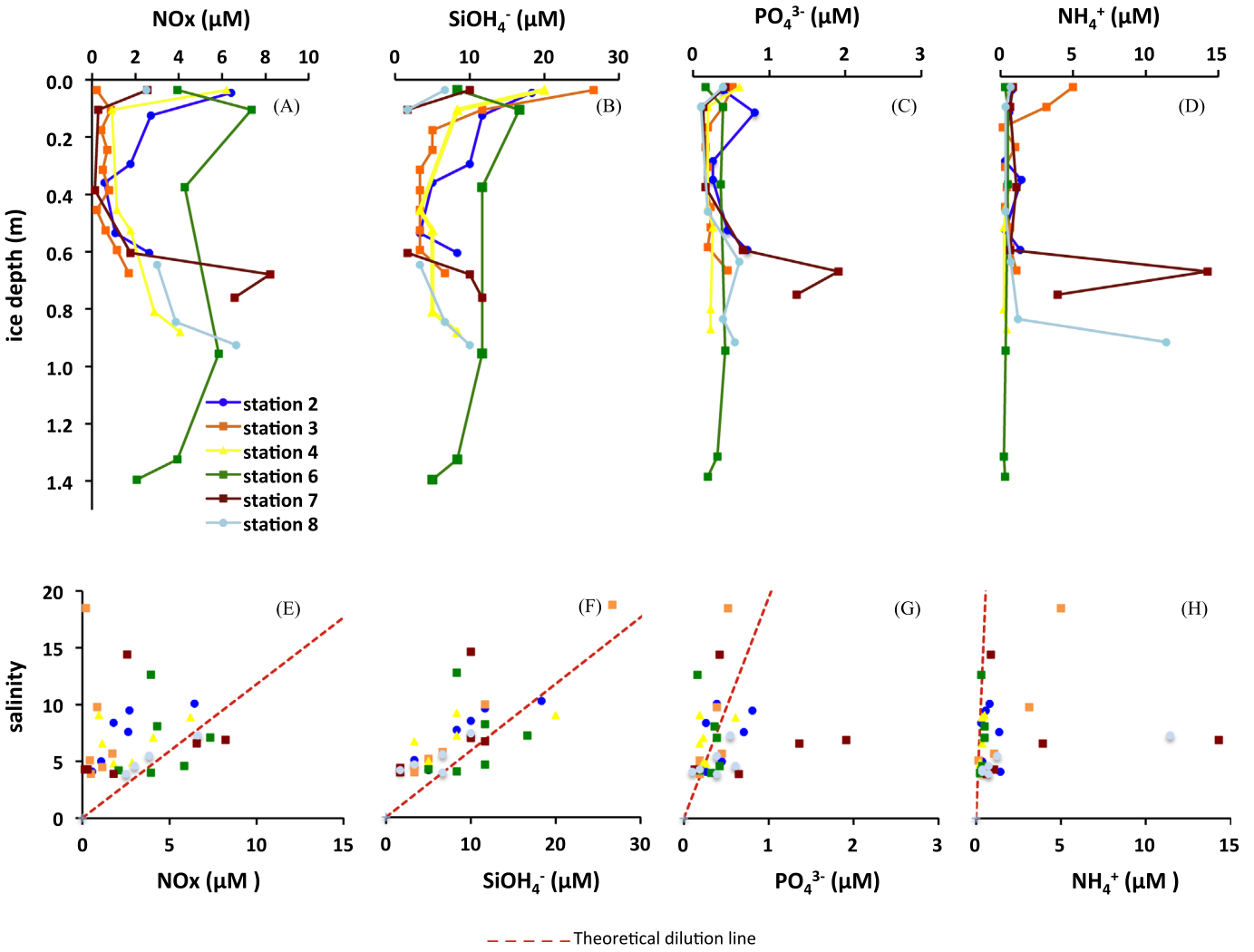

Fig. 4. Upper panel: concentrations (μM) in (A) nitrate+nitrate (NO_x), (B) silicic acid ($SiOH_4^-$), (C) phosphates (PO_4^{3-}) and (D) ammonium (NH_4^+), as a function of sea ice depth (m) during SIPEX-2. Lower panel: sea ice concentrations of (E) nitrate+nitrate (NO_x), (F) silicic acid ($SiOH_4^-$), (G) phosphate (PO_4^{3-}) and (H) ammonium (NH_4^+), plotted against salinity. The red dotted line represents the theoretical dilution line. (For interpretation of the references to color in this figure legend, the reader is referred to the web version of this article.)

Particulate organic carbon and PON concentrations in sea ice ranged, respectively, between 24 and 1088 μg/L (average 332 ± 298 μg/L) and between 2 and 156 μg/L (average 42 ± 41 μg/L). Similar to Chl*a* and DOC, the POC and PON maxima did not occur at the ice/water interface (Fig. 5C and D). In the top most and lower most sections of the ice cover, the POC:PON ratios were lower and close to the Redfield C:N molar ratio of 6.6 mol:mol typical of phytoplankton (Redfield, 1958). These ice sections therefore harbor autotrophic activity.

Significant correlations were observed between POC and PON, and PO_4^{3-} and Chl*a* across all sites (Table 3). Chlorophyll *a* also correlated significantly with PON, NH_4^+ and PO_4^{3-}.

3.2.2. Iron distributions

Fig. 6 shows the profiles of DFe and PFe concentrations in collected sea-ice cores. The DFe profiles are highly variable both between stations and within profiles. The PFe profiles differ greatly between sampling sites, with stations 7 and 8 noticeably different. The ranges in sea ice were 0.9–17.4 nM DFe (average 7.5 ± 4.5 nM) and 0.04–990 nM PFe (average 133 ± 215 nM). Similar to previous Antarctic studies, our results show high DFe concentrations in sea ice relative to under-ice seawater (range 0.09–3.05 nM DFe; 15–1000 m deep; Schallenberg et al., this issue). Significant correlations between DFe and V_b/V (R=0.55) and DFe and PFe (R=0.57) were observed (Table 3).

The fractional solubility of Fe (FS–Fe=ratio of dissolved to total Fe concentration) in sea ice varied between 0.01 and 0.98 (average FS–Fe=0.13 ± 0.16).

Based on the data collected at 6 sections within each core, we vertically integrated the concentrations of DFe and PFe at each station (Table 4). We also applied this integration to POC and Chl*a* concentrations. Depth integrated DFe was the highest at station 6 (16.9 μmol/m^2) and the lowest at station 3 (2.2 μmol/m^2). Depth integrated PFe was the highest at station 7 (294.3 μmol/m^2) and the lowest at station 3 (16 μmol/m^2). Station 7 also exhibited the highest depth integrated Chl*a* (3.6 mg/m^2) and POC (660 mg/m^2) concentrations.

4. Discussion

4.1. Sea-ice physical properties

Based on the ice temperatures and brine volume ratios in Fig. 3, three seasonal regimes during SIPEX-2 can be identified: station 3 was a cold winter station, station 4 a transition station, and the

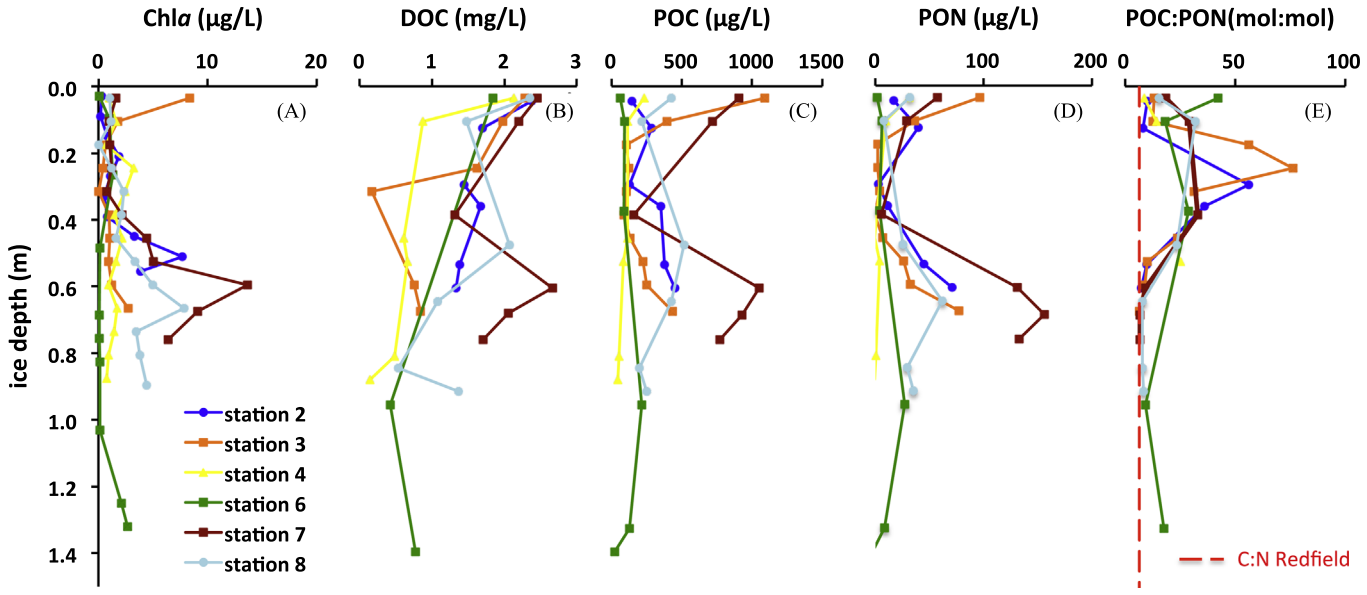

Fig. 5. Concentrations (µg/L) in (A) chlorophyll *a* (Chl*a*), (B) dissolved organic carbon (DOC), (C) particulate organic carbon (POC), (D) particulate organic nitrogen (PON) and (E) POC:PON ratios (mol:mol) as a function of sea-ice depth (m) during SIPEX-2. The red dotted line represents the C:N Redfield molar ratio (106:16). (For interpretation of the references to color in this figure legend, the reader is referred to the web version of this article.)

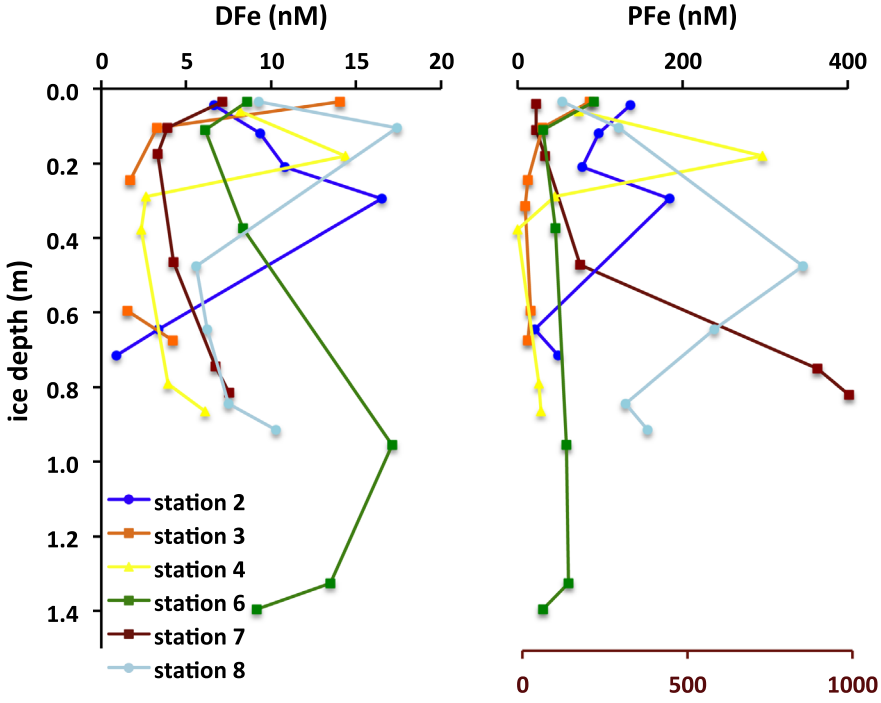

Fig. 6. Concentrations (in nM) in dissolved and particulate iron (DFe and PFe) as a function of sea-ice depth (in m) during SIPEX-2. The lower *x*-axis is the scale for PFe at station 7.

Table 4
Depth integrated concentrations of Fe (in µmol/m^2), Chl*a* and POC (in mg/m^2) in sea ice during SIPEX-2

stations	DFe	PFe	Biogenic PFe	Lithogenic PFe	Chl*a*	POC
2	6.6	73.4	56.6	16.7	2.3	230.7
3	2.2	16.0	10.0	6.0	1.3	233.7
4	4.9	57.2	44.8	12.4	1.2	90.3
6	16.9	74.9	28.1	47.9	1.2	190.2
7	4.3	294.3	250.0	44.3	3.6	657.4
8	8.9	197.0	89.7	107.3	3.0	339.5
Average	7.3	118.8	79.9	39.1	2.1	290.3
Stdev	5.2	105.1	87.6	37.6	1.1	197.0

other four stations were warm spring type stations. The increase in the mean air temperature most likely triggered the warming of the ice, from the top, as exemplified for stations 3, 4, 6 and 7 (Fig. 3A). Although the mean air temperatures at stations 2 and 8 were low, the in situ ice temperatures were relatively warm. The thick snow cover at station 8 probably insulated the sea ice from the cold atmospheric conditions. The snow layer was however thin at station 2. This suggests that the air temperature decreased recently and did not have time to affect the ice temperatures before we collected the samples.

Ice textures were dominated by granular ice, which highlights the presence of either snow ice or frazil ice crystals. Frazil ice

forms under dynamic turbulent conditions at high growth rates, concentrating micro-organisms (living and detrital) by nucleation of frazil ice crystals or by scavenging cells as frazil crystals float up through the water column (Garrison et al., 1989; Horner, 1996). Precipitation of snow and its redistribution through drifts are key features of the Antarctic pack ice zone (Sturm and Massom, 2010). Snow layers accumulate on top of the ice cover soon after its formation. Depending on the sea-ice thickness below, the snow cover may become thick enough to depress the sea-ice cover and seawater may then infiltrate into the snow pack. "Snow ice" then forms by refreezing of the flooded snow and creates a solid layer of ice on top of the ice floe, which is of granular type (Worby et al., 1998). Snow ice may then be underlain by frazil ice, which is also granular. Columnar ice forms slowly compared to granular ice (Eicken, 2003), and tends to efficiently reject micro-organisms in the early stage of ice growth (Palmisano and Garrison, 1993; Weissenberger and Grossmann, 1998). In our samples, no clear relationship between biological occurrence or Fe and ice textures was observed.

Ice texture observations suggest that the ice collected at stations 3 and 4 grew thermodynamically (i.e. due to a decrease in ambient temperature). Station 6 grew in thickness because of dynamic processes including rafting (where ice floes raft on top of each other) and ridging (blocks of ice are pushed onto, and below, the edge of ice floes). The repeated observation of deformed columnar ice crystals supports this rafting process. As a result, the ice core collected at station 6 which was subjected to rafting was thicker than at station 3 where the ice grew thermodynamically. The snow layer was thick throughout our study, leading to snow ice formation at several stations. Station 4 displayed 0.16 m of snow ice, underlain by 0.13 m of frazil ice, and then columnar ice. This is confirmed by the in situ ice temperatures and salinity for station 4 where the top 0.16 m of snow ice were warmer and saltier than the sea ice below (Fig. 3A and B). Snow ice also likely formed at the snow-ice interface at stations 6, 7 and 8 (Fig. 2). We did not measure $\delta^{18}O$ at the trace metal sampling sites to decipher snow ice from frazil ice. $\delta^{18}O$ was measured in sea ice by other research groups at the main sampling sites during SIPEX-2 and do highlight the recurrence of snow ice formation on their sites (Heil et al., 2016). We consider the same feature applies to the entire ice floes studied, including the trace metal sampling sites.

4.2. Biogeochemical comparison to previous studies: DFe and DOC thresholds in sea ice

The 24–1088 μg/L POC concentrations from SIPEX-2 were lower than the 28–4784 μg/L measured during ARISE (Becquevort et al., 2009) and 38–3309 μg/L during SIPEX-1 (van der Merwe et al., 2009) in the same sector, at the same time of the year. The POC:PON ratios were generally close to the Redfield ratio in bottom ice but elevated in the internal ice sections. This could be explained by the relative dominance of carbon associated with exopolysaccharides (EPS) over carbon associated with autotrophs in these ice layers (Ugalde, 2016). Exopolysaccharides are commonly enriched in carbon relative to nitrogen when compared to the Redfield ratio (26 mol:mol; Engel and Passow, 2001). However the very high POC:PON ratios observed in internal layers (up to 76 mol:mol at station 3, Fig. 5E) could reflect the extremely low PON concentrations (Fig. 5D) due to nitrogen limitation in these sections (Fig. 4A).

Unlike SIPEX-1 (van der Merwe et al., 2009), DOC did correlate significantly with POC ($R=0.67$) and PON ($R=0.51$) during SIPEX-2. The significant correlation between DOC and POC could indicate an algal origin for sea ice DOC, as previously observed during spring blooms in the Arctic (Bunch and Harland, 1990; Smith et al., 1997; Riedel et al., 2008). However, the measured DOC:POC ratio in sea ice averaged 7:1 (range of 1:1 to 32:1) which is lower than the mean global ocean value of 15:1 (Millero, 1996; Kepkay, 2000). One explanation may be an abiotic transformation of DOC into POC when a DOC threshold is reached (Becquevort et al., 2009). This transfer of DOC into POC would also explain the significance of the relationship observed in our study between DOC and POC (Table 3).

The DFe measured during SIPEX-2 (DFe=0.9–17.4 nM) was within the ranges reported during ARISE (DFe=2.1–26.1 nM; Lannuzel et al., 2007) and SIPEX-1 (DFe=0.2–14.4 nM; van der Merwe et al., 2011a) which were studies located in the same sector and at the same time of the year. Therefore, although the sea ice conditions were very different in 2003, 2007 and 2012, the DFe interannual variability in late austral winter-spring seems low. Sea-ice thickness, texture and growth (i.e. thermodynamic versus dynamic) do not seem to control the concentrations of DFe in sea ice. One hypothesis is that the sources of new and regenerated DFe are very similar from one year to the other. Fast ice however, does not incorporate much more DFe than pack ice (Lannuzel et al., 2010), even when new sources of Fe are only a few tens of meters away from the collected ice (van der Merwe et al., 2011b). Another hypothesis is that DFe reaches a maximum concentration threshold in sea ice, which it cannot exceed. This would explain the lack of spatial variability in DFe concentrations between pack ice stations during SIPEX-2 (Fig. 6), and between pack-ice and fast-ice sites collected around Antarctica (Lannuzel et al., 2010). Similar to DOC and POC, DFe and PFe were also significantly correlated in sea ice during SIPEX-2 ($R=0.57$, $n=36$, $p<0.01$). We suggest that once a threshold is reached for the apparent DFe concentration in the brine channels, DFe is transformed into PFe. This theory is further supported by the low fraction of DFe relative to PFe concentrations typically encountered in sea ice (FS–Fe=0.13 in pack ice and FS–Fe=0.03 in fast ice) compared to open waters (FS–Fe=0.52 ± 0.19, $n=31$, calculated from 0 to 150 m, SAZ-SENSE data published in Lannuzel et al. (2011)). This process is similar to what would happen in seawater, however the PFe cannot sink out in sea ice and therefore lead to the high PFe relative to DFe. To get an estimate of the DFe threshold value within the brine channels, we calculate the potential brine DFe concentrations as follows:

$$DFe_{brine} = \frac{DFe_{bulk} \times brinesalinity}{bulksalinity},$$

where DFe_{bulk} is the concentration of DFe in the melted ice section, bulk salinity is the salinity of the melted ice section and brine salinity is calculated as a function of bulk ice salinity and in situ temperature in that sea ice section.

Our DFe_{brine} concentrations however, do not reach a clear threshold number (DFe_{brine} range=6.8–173.7 nM and average=55.1 ± 39.0 nM). Biological uptake and remineralization, as well as organic ligand concentrations may control the equilibrium between the dissolved and particulate phase, and therefore shift the solubility threshold value. Recent work in Antarctic fast ice has shown a linear relationship between DFe and organic ligands (Lt) concentrations in sea-ice and brine samples, with [Lt]=0.90 [DFe]+4.24 in sea ice ($R^2=0.93$, $n=34$) and [Lt]=1.08 [DFe]+4.86 in brines ($R^2=0.98$, n=12). These results suggest that organic ligands control the concentrations of DFe in sea ice. Once the ligands become saturated with Fe, non-organically bound DFe become scavenged onto particles (Lannuzel et al., under review).

In the case of PFe, the ranges measured during ARISE in 2003 (PFe=2.0 –96.6 nM; Lannuzel et al., unpublished data) and SIPEX-1 in 2007 (PFe=0.9–217.7 nM; van der Merwe et al., 2011a) were much lower than SIPEX-2 in 2012 (PFe=0.04–990 nM). The highest PFe concentrations were observed at station 7 (Fig. 6), which is the closest station to drifting icebergs and the continental shelf. Note that the range from SIPEX-1 in 2007 includes one fast-ice

station, for which the PFe concentration was anomalously high at 217.7 nM. Fast ice typically incorporates more lithogenic PFe than pack ice because of its proximity to continental sources (Grotti et al., 2005; van der Merwe et al., 2011a,b; Lannuzel et al., 2014).

4.3. Lithogenic and biogenic particulate Fe

4.3.1. Icebergs

Several icebergs were sighted in the area (Fig. 1). Icebergs C28B, B16, B09F and B09G remained on the continental shelf during the SIPEX-2 expedition and we suggest that their influence on our ice stations was therefore minimal. However, Fig. 1 shows that iceberg B09D closely followed the shelf break during our study, suggesting it may have dragged along the shelf and stirred some sedimentary PFe in its path. Station 7 being within 30 km and directly in the lee of the B09D, the iceberg could have contributed to the incorporation of dissolved and particulate Fe into the sea-ice cover, either by direct melting or by stirring up some sediments (Raiswell et al., 2008). No under ice seawater PFe samples were collected during SIPEX2 to support this hypothesis. The under-ice seawater profiles did not indicate that B09D influenced the DFe concentrations at station 7 (Schallenberg et al., 2016). Note that the sea-ice data are difficult to directly compare to the under-ice seawater Fe data presented in Schallenberg et al. (2016). This is because sea-ice and seawater datasets are somewhat decoupled; i.e. sea ice collected at station 7 does not necessarily originate from the same location as seawater collected at station 7.

4.3.2. Lithogenic and biogenic contributions to PFe

One method to evaluate the lithogenic contribution to sea ice is to compare the Fe/Al ratios in collected samples to the Fe/Al ratios reported in lithogenic samples from the literature or from specific locations relevant to the study. Fig. 7 shows that the molar ratios Fe/Al (1.15 ± 0.93, $n=30$) in all pack-ice samples are above the crustal and sedimentary ratios of respectively 0.33 (Taylor, 1964) and 0.26–0.34 (Angino, 1969; Gasparon et al., 2007). This suggests that the PFe found in these pack-ice samples cannot be solely from atmospheric deposition and resuspended sediments. High fast ice Fe/Al ratios were observed by de Jong et al. (2013) when Chl*a* concentrations exceeded a threshold (>0.5 μg/L), suggesting a biogenic modification of the elemental ratios in the bottom ice. We further investigate relative lithogenic and biogenic contributions.

Assuming that Al is solely of lithogenic origin and using the mean crustal Fe/Al molar ratios typical of lithogenic samples (Fe/Al=0.33; Taylor, 1964), it is possible to calculate the lithogenic and biogenic PFe concentrations in sea ice (Frew et al., 2006).

$$[\mathrm{PFe}]_{\mathrm{lithogenic}} = [\mathrm{PAl}]_{\mathrm{ice}} \times 0.33$$

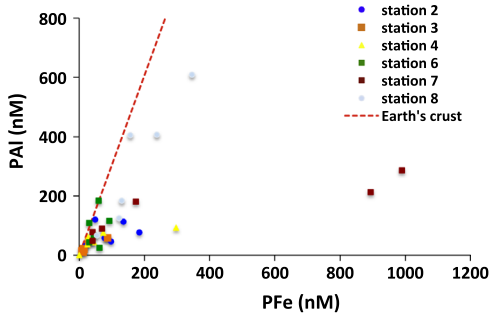

Fig. 7. Plot of particulate Fe (PFe) versus particulate Al (PAl) concentrations (in nM). Earth's crustal Fe/Al ratio=0.33 mol:mol is indicated by the red dotted line. (For interpretation of the references to color in this figure legend, the reader is referred to the web version of this article.)

$$[\mathrm{PFe}]_{\mathrm{biogenic}} = [\mathrm{PFe}]_{\mathrm{ice}} - [\mathrm{PFe}]_{\mathrm{lithogenic}}$$

The results show that 29% of PFe was lithogenic in origin (with $[\mathrm{PFe}]_{\mathrm{lithogenic}} = 35 \pm 40$ nM, $n=30$). Assuming that biogenic PFe is the difference between the total PFe and lithogenic PFe, then the concentration of biogenic PFe in pack ice was on average 93 ± 200 nM ($n=30$), which represents 71% of total PFe. The biogenic contribution represents 87% at station 7, which was the highest recorded on the voyage. This is consistent with POC and Chl*a* data which were also the highest at station 7 (Table 4). Rates of primary productivity in sea ice at station 7 were the second highest during the voyage with an average of 3.32 mg/C/m^2/d (range 0.04–5.5 mg/C/m^2/d), most of which was associated with the internal algal community (Roukaerts et al., 2016).

The concentrations of PFe in pack ice in the same sector were much lower in 2003 (2.0–96.6 nM; Lannuzel et al., unpublished data) and 2007 (0.9–77.7 nM; van der Merwe et al., 2011a) than in 2012 (0.04–990 nM; this study). When using the PFe and PAl concentrations measured in 2007, we find that the biogenic PFe concentrations varied greatly between 2007 (0.0–33.9 nM) and 2012 (0.0–895.5 nM). The high biogenic PFe concentrations recorded during SIPEX-2 illustrates the bio-accumulation of Fe in sea ice, potentially because of differences in the water column characteristics where/when sea ice formed in 2012. The bio-accumulation of Fe could be due to: (1) high DFe inputs originating from the continental shelf or icebergs (Schallenberg et al., 2016) being then actively taken up by sea-ice algae at the ice/water interface and transferred into PFe (Lannuzel et al., 2007; van der Merwe et al., 2011a), or (2) biogenic PFe directly incorporated in sea ice when it originally formed further East potentially on the continental shelf where productivity (and therefore biogenic PFe) may have been higher.

4.4. Role of seasonal sea ice as a natural ocean fertilizer

When using the depth integrated DFe, lithogenic PFe and biogenic PFe concentrations in East Antarctic pack ice from Table 4, and assuming a 1 m thick ice cover and 30 days of melting, the estimated Fe flux from melting pack ice to East Antarctic surface waters in spring 2012 would be 0.2 μmol/m^2/d for DFe, 2.7 μmol/m^2/d for biogenic PFe and 1.3 μmol/m^2/d for lithogenic PFe. Therefore, our study highlights that the biogenic and lithogenic PFe fluxes are an order of magnitude higher than the DFe flux. Particulate organic matter associated with Fe (=biogenic PFe) can be oxidized or remineralized, and release Fe into the dissolved phase, together with carbon, nitrogen and silicate. Remineralization processes have been recognized to play a major role in supplying available Fe to the phytoplankton community (Hurst and Bruland, 2007; Hutchins and Bruland, 1994). The flux of biogenic PFe released from sea ice being 10 times higher than the DFe flux. The importance of sea ice in supplying bio-available PFe to the Antarctic surface waters therefore cannot be ignored. If only 10% of biogenic PFe is regenerated, bio-available PFe can match the DFe flux, therefore doubling the flux of bio-available Fe supplied by melting sea ice to Antarctic surface waters. Iron associated with lithogenic material can also become bio-available, but to a much lesser extent than the biogenic fraction. The size and density of the particles, concentration of organic ligands, ocean mixing, rate of grazing by higher trophic levels and remineralization processes will control the concentration of bio-available PFe supplied by sea ice to surface waters.

Several DFe fluxes have been put forward in the Southern Ocean, and highlight that atmospheric dust input (continental + extraterrestrial) onto pack ice is generally low (i.e. 0.0016 μmol/m^2/d; from Lannuzel et al., 2007). Apart from regional exceptions, it is ack-

nowledged that the main source of Fe to Antarctic sea ice comes from below, either by entrainment from the mixed layer (=new+regenerated Fe) or from organic matter and associated Fe (=regenerated Fe) left floating in seawater from the preceding summer season (Lannuzel et al., 2010). Modeling studies have reported that diapycnal diffusion supplies to the Southern Ocean 0.0016–0.0157 μmol/m^2/d of DFe while deep winter mixing supplies 0.026–0.091 μmol/m^2/d (Tagliabue et al., 2014). With 0.2 μmol DFe /m^2/d released to Antarctic surface waters during the melt season, sea ice supplies more DFe than all the other mentioned sources put together. As sea ice covers 40% of the Southern Ocean, its role as a natural ocean fertilizer therefore cannot be ignored.

4.5. Sea-ice biogeochemistry during SIPEX-2: Iron versus light limitation

Due to favorable environmental conditions at the bottom of ice floes, ice algal communities typically develop at the ice/water interface, resulting in maximum Chl*a*, POC and PON, and a characteristic "L-shaped" vertical profile. However, surface flooding can result in accumulation of biogenic particulate matter in surface slush layers, leading to C-shaped profiles (Meiners et al., 2012). East Antarctic sea ice has been reported to harbor primarily bottom communities (Grose and McMinn, 2003; Meiners et al., 2011). Interestingly, this was not the case in our study. The complex sea-ice properties and ice growth mentioned earlier in the discussion led to heterogeneous distributions of Chl*a*, DOC, POC, PON and to a lesser extent macro-nutrient concentrations (Figs. 4 and 5).

Silicic acid did follow a conservative model of incorporation in sea ice i.e. in proportion with salinity gradients, whilst the other nutrients were either enriched (NH_4^+ and PO_4^{3-}) or consumed (NO_x and PO_4^{3-}) in sea ice. Stations 3 and 7 exhibited enhanced Chl*a*, POC and PON concentrations at the top of the ice cover, suggesting an active surface community. Station 7 displayed a 0.35 m thick snow cover on top of 0.72 m of granular ice (Fig. 2), suggesting some snow ice formed in the top of the ice cover and therefore some surface flooding occurred. The infiltration of seawater may have seeded the surface of the ice with nutrients and micro-organisms, leading to an active surface community at station 7 with a C:N close to the Redfield ratio and high POC, PON and Chl*a* (Fig. 5). In contrast, it is unclear at this stage what lead to the high POC and Chl*a* observed at station 3 in the top layer of the sea ice. The snow thickness was amongst the lowest measured during SIPEX-2 (0.25 m), the ice textures highlight thermodynamic growth (undeformed and level ice) and no snow ice formation. Furthermore, the ice temperatures and brine volumes indicate that the ice cover was typical of winter conditions. We suggest that the relatively thin snow cover led to increased light availability at station 3 compared to other sampling sites, which led to the development of a surface community which used the available nutrients initially incorporated during the early stage of sea-ice formation. This is exemplified by the complete drawdown in NO_x at the ice/snow interface (Fig. 4A and F), compared to the other ice stations where seawater infiltration replenished the surface community with macro-nutrients. However, the $SiOH_4^-$ concentration remained the highest at station 3 (Fig. 4B), suggesting the community developing was not dominated by diatoms, but most likely *Phaeocystis* such as *P. Antarctica* or *P. globulosa*. Interestingly, relatively high NH_4^+ concentrations observed at station 3 suggest strong recycling processes in surface sea ice (Fig. 4D), which supplied regenerated nitrogen needed for the autotrophic community to maintain growth rates. However, resupply of new NO_x through seawater infiltration, either by percolation or flooding, would be required for biomass to increase while maintaining Redfield stoichiometry.

Rates of primary production were measured using stable isotope uptake incubations on the trace metal site at stations 2, 3, 4, 6 and 7 (Roukaerts et al., 2016). The highest rates were measured at station 2 (5.5 mg/C/m^2/d) followed by station 7 (3.3 mg/C/m^2/d). Station 4 had the lowest rates of primary productivity (0.04 mg/C/m^2/d), in agreement with the low Chl*a*, POC and PON concentrations measured in sea ice at that station. A clear increase in primary production was observed during the one-month expedition, during which the daylight increased by about 3 h. Although we do observe an increase in C uptake rates as the season progresses, the levels are low and characteristic of pre-bloom conditions (Roukaerts et al., 2016).

Overall the availability of macro-nutrients and DFe was high throughout the study (i.e. non limiting concentrations except for NO_x < 0.2 μM at stations 3 and 7 in certain sections) and the warm ice temperatures and high permeability of the ice cover were favorable for algal growth. However, a common feature was the thick snow cover on top of the ice at most stations. This feature, on one hand, led to seawater infiltration which may have favored the growth of surface communities, but on another hand, may have restricted incoming light reaching the bottom communities. An increase of snow thickness by 0.2 m can restrict light transmission through sea ice by up to 80% (Arrigo, 2003). In our study, snow thickness averaged 0.4 m and represented almost 30% of the sea-ice thickness. We therefore suggest that, because of extensive snow cover witnessed during the expedition, the low light levels led to the low sea-ice primary productivity (see also Ugalde et al., 2016; Roukaerts et al., 2016).

The Fe demand of sea-ice algae can be estimated from cellular Fe:C and primary productivity (PP) (Fe_{demand} = new PP × $(Fe:C)_{cellular}$) where new PP = 0.5–6 mg/C/m^2/d (Roukaerts et al., 2016). To the best of our knowledge, no data on intracellular Fe:C ratios currently exist for sea-ice algae assemblages. In seawater, this ratio typically ranges from 10 to 40 μmol Fe:mol C (de Baar et al., 2008; Hassler and Schoemann, 2009; Sarthou et al., 2005) and not only does it vary in space and time, but it also varies with the type of phytoplankton. Iron fertilized sites tend to sit in the higher range of $(Fe:C)_{cellular}$ ratios (Sarthou et al., 2005). Using a conservative estimation of $(Fe:C)_{cellular}$ = 10–40 μmol:mol for sea ice algae, we obtain an Fe_{demand} = 0.4–20 nmol/m^2/d in sea ice. This Fe_{demand} is well below the DFe_{supply} in sea ice = 0.86 μmol/m^2/d estimated during the voyage, confirming that Fe did not limit the primary productivity in sea ice at this time of year. The DFe_{supply} in sea ice was approximated by substracting the lowest from the highest DFe inventory values reported in table 4 (=16.9–2.2 μmol/m^2), and dividing by the time elapsed between these 2 stations (17 days).

If the growth of the sea-ice community was not directly controlled by the lack of Fe, the under ice phytoplankton community may however have been limited by Fe supply later in the season, when light limitation was alleviated. In the marginal ice zone, a 0.2 μmol/m^2/d supply of DFe from melting pack ice and $(Fe:C)_{cellular}$ = 10–40 μmol:mol would sustain a gross primary productivity of 0.06–0.24 g/m^2/d in the East Antarctic sector. Our Fe-induced productivity estimate represents 10% to 40% of the 0.61 g/m^2/d measured in seawater in the marginal ice zone in spring 1996 (Nicol et al., 2000). The higher and lower ends of our estimate are controlled by the Fe:C range we used, which is based on phytoplankton cultures and therefore may not match the in situ ratios. Additionally, if 10% to 70% of biogenic PFe supplied from sea ice is soluble and therefore becomes available for phytoplankton uptake, then the Fe fertilization from sea ice can fully account for the primary productivity value reported by Nicol et al. (2000). Our estimates clearly demonstrate that the uncertainties on the intracellular Fe:C ratios and on the solubility of PFe have to be addressed before we can fully appreciate the role of sea ice-bearing Fe in controlling primary productivity in the marginal ice zone.

5. Conclusion

Concentrations of DFe in pack ice collected during SIPEX-2 were 2 to 3 orders of magnitude more concentrated than in ice-free East Antarctic waters (Schallenberg et al., 2016). The SIPEX-2 DFe ranges were found to lie between those previously reported from the ARISE and SIPEX-1 studies, even though the sea-ice conditions were very different. Sea-ice thickness, texture and growth (i.e. thermodynamic versus dynamic) do not control the concentrations of DFe in sea ice. Instead, we hypothesize that DFe precipitates into PFe when it reaches a certain in situ solubility threshold. This threshold may be controlled by the concentration of Fe-binding organic ligands present in sea ice. Particulate Fe concentrations did vary between stations, with station 7 displaying unique characteristics. A strong biogenic PFe signature was observed at all stations, especially at station 7. Iron supply estimates highlight the dominance of PFe over DFe in fertilizing the marginal ice zone, but questions remain regarding how bio-available PFe may become once released into seawater. The flooding and dynamic conditions under which sea ice grew during SIPEX-2, involving rafting and ridging processes, led to unusual biogeochemical profiles in sea ice. The availability of nutrients, favorable sea-ice conditions (warm and porous), low primary productivity and thick snow covers observed throughout the study suggest that light was the primary factor limiting growth in sea ice at this time of the year in the SIPEX-2 study area.

Acknowledgements

The authors would like to thank the officers and crew of the *RV Aurora Australis* for their logistic support during the SIPEX-2 voyage. We would like to acknowledge Olivier Lecomte for helping in the collection of the trace metal ice cores. This work was co-funded by the Australian Research Council (LE0989539 and DE120100030), the Australian Government Cooperative Research Centres Programme through the Antarctic Climate & Ecosystems (ACE CRC) and the Australian Antarctic Science (AAS) project no. 4051.

References

Angino, E.E., 1969. Geochemistry of Antarctic pleagic sediments. Geochim. Cosmochim. Acta 30, 939–961.

Arndt, J.E., Schenke, H.W., Jakobsson, M., Nitsche, F., Buys, G., Goleby, B., Rebesco, M., Bohoyo, F., Hong, J.K., Black, J., Greku, R., Udintsev, G., Barrios, F., Reynoso-Peralta, W., Morishita, T., Wigley, R., no date. The International Bathymetric Chart of the Southern Ocean (IBCSO) Version 1.0—a new bathymetric compilation covering circum-Antarctic waters, Geophys Res. Lett., http://dx.doi.org/10.1002/grl.50413.

Arrigo, K.R., 2003. Physical control of chlorophyll *a*, POC, and TPN distributions in the pack ice of the Ross Sea, Antarctica. J. Geophys. Res. 108 (C10), 3316. http://dx.doi.org/10.1029/2001JC001138.

Becquevort, S., Dumont, I., Tison, J.L., Lannuzel, D., Sauvée, M.L., Chou, L., Schoemann, V., 2009. Biogeochemistry and microbial community composition in sea ice and underlying seawater off East Antarctica during early spring. Polar Biol. 32 (6), 879–895. http://dx.doi.org/10.1007/s00300-009-0589-2.

Blain, S., Quéguiner, B., Armand, L., Belviso, S., Bombled, B., Bopp, L., Wagener, T., 2007. Effect of natural iron fertilization on carbon sequestration in the Southern Ocean. Nature 446 (7139), 1070–1074. http://dx.doi.org/10.1038/nature05700.

Bowie, A.R., Townsend, A.T., Lannuzel, D., Remenyi, T., van der Merwe, P., 2010. Modern sampling and analytical methods for the determination of trace elements in marine particulate material using magnetic sector inductively coupled plasma-mass spectrometry. Anal. Chim. Acta 676 (1-2), 15–27. http://dx.doi.org/10.1016/j.aca.2010.07.037.

Boyd, P.W., Law, C.S., Wong, C.S., Nojiri, Y., Tsuda, A., Levasseur, M., 2004. The decline and fate of an iron-induced subarctic phytoplankton bloom. Nature 428, 549–553. http://dx.doi.org/10.1029/2001JB001129.

Boyd, P.W., Jickells, T., Law, C.S., Blain, S., Boyle, E.a., Buesseler, K.O., Watson, AJ, 2007. Mesoscale iron enrichment experiments 1993–2005: synthesis and future directions. Science (New York, NY) 315 (5812), 612–617. http://dx.doi.org/10.1126/science.1131669.

Bunch, J.N., Harland, R.C., 1990. Bacterial production in the bottom surface of sea ice in the Canadian subarctic. Can J. Fish. Aquat. Sci. 47, 1986–1995.

Cox, G.F.N., Weeks, W.F., 1983. Equations for determining the gas and brine volumes in sea-ice samples. Ann. Glaciol. 29 (102), 306–316.

de Baar, H.J.W., Buma, A.G.J., Nolting, R.F., Cadée, G.C., Jacques, G., Tréguer, P., 1990. On iron limitation of the Southern Ocean: experimental observations in the Weddell and Scotia Seas. Mar. Ecol. Prog. Ser. 65, 105–122.

de Baar, H.J.W., Gerringa, L., Laan, P., Timmermans, K., 2008. Efficiency of carbon removal per added iron in ocean iron fertilization. Mar. Ecol. Prog. Ser. 364, 269–282. http://dx.doi.org/10.3354/meps07548.

de Jong, J., Schoemann, V., Maricq, N., Mattielli, N., Langhorne, P., Haskell, T., Tison, J., 2013. Iron in land-fast sea ice of McMurdo Sound derived from sediment resuspension and wind-blown dust attributes to primary productivity in the Ross Sea, Antarctica. Mar. Chem. , http://dx.doi.org/10.1016/j.marchem.2013.07.001.

Eicken, H., 2003. From the microscopic to the macroscopic to the regional scale, growth, microstrucutre and properties of sea ice. In: Sea Ice – an Introduction to Its Physics, Biology, Chemistry and Geology. Blackwell Science, London, pp. 22–81.

Engel, A., Passow, U., 2001. Carbon and nitrogen content of transparent exopolymer particles (TEP) in relation to their Alcian Blue adsorption. Mar. Ecol. Prog. Ser. 219, 1–10.

Frew, R.D., Hutchins, D., Nodder, S., Sanudo-Wilhelmy, S., Tovar-Sanchez, A., Leblanc, K., Boyd, P.W., 2006. Particulate iron dynamics during FeCycle in subantarctic waters southeast of New Zealand, Global Biogeochem CyBiogeochem. Cycles 20 (1), http://dx.doi.org/10.1029/2005GB002558, (n/a–n/a)!.

Garrison, D.L., Close, A.R., Reimnitz, E., 1989. Algae concentrated by frazil ice: evidence from laboratory experiments and field measurements. Antarct. Sci. 1 (4), 313–316.

Gasparon, M., Ehrler, K., Melles, M., 2007. Temporal and spatial variability of geochemical backgrounds in the Windmill Islands, East Antarctica: implications for climatic changes and human impacts. Appl. Geochem., *22*; , pp. 888–905. http://dx.doi.org/10.1016/j.apgeochem.2006.12.018.

Golden, K., Ackley, S.F., Lytle, V., 1998. The percolation phase transition in sea Ice. Science (New York, NY) 282 (5397), 2238–2241 (Retrieved from).

Grose, M., McMinn, A., 2003. Algal biomass in east Antarctic pack ice: how much is in the east. In: Huiskes, A.H.L., Gieskes, W.W.C., Rozema, J., Schorno, R.M.L., van der Vies, S.M., Wolff, W.J. (Eds.), Antarctic Biology in a Global Context. Proceedings of the VIIIth SCAR International Biology Symposium. Backhuys Publishers, Leiden, pp. 21–25.

Grotti, M., Soggia, F., Ianni, C., Frache, R., 2005. Trace metals distributions in coastal sea ice of Terra Nova Bay, Ross Sea, Antarctica. Antarct. Sci. 17 (2), 289–300. http://dx.doi.org/10.1017/S0954102005002695.

Hassler, C.S., Schoemann, V., 2009. Bioavailability of organically bound Fe to model phytoplankton of the Southern Ocean. Biogeosci. Discuss. 6, 1677–1712.

Heil, Hutchings, Massom, Stevens, Lecomte et al., 2016. Physical Characterization of the East Antarctic Pack Ice During SIPEX 2012. Deep Sea Res. Part II, 131, 7–21.

Horner, R., 1996. Ice algal investigations:historical perspective. In: NIPR Symp. Polar Biol., 1–12.

Hurst, M.P., Bruland, K.W., 2007. An investigation into the exchange of iron and zinc between soluble, colloidal, and particulate size-fractions in shelf waters using low-abundance isotopes as tracers in shipboard incubation experiments. Mar. Chem. 103 (3-4), 211–226. http://dx.doi.org/10.1016/j.marchem.2006.07.001.

Hutchins, D.A., Bruland, K.W., 1994. Grazer-mediated regeneration and assimilation of Fe, Zn and Mn from planktonic prey. Mar. Ecol. Prog. Ser. 110, 259–269.

Kepkay, P.F., 2000. Colloids and the ocean carbon cycle. In: Wangersky, P. (Ed.), The Handbook Of Environmental Chemistry, vol 5. Part D: Marine Chemistry. Springer, Berlin, pp. 35–56.

Lancelot, C., Montety, A., De, Goosse, H., Becquevort, S., Schoemann, V., 2009. Spatial distribution of the iron supply to phytoplankton in the Southern Ocean: a model study. Biogeosci. Discuss. 6, 4919–4962.

Langway, C.C., 1958. Ice Fabrics and the Universal Stage. USA Cold Regions Research and Engineering Laboratory, CRREL Technical Report, 62, .

Lannuzel, D., de Jong, J., Schoemann, V., Trevena, A., Tison, J.-L., Chou, L., 2006. Development of a sampling and flow injection analysis technique for iron determination in the sea ice environment. Anal. Chim. Acta 556 (2), 476–483. http://dx.doi.org/10.1016/j.aca.2005.09.059.

Lannuzel, D., Schoemann, V., de Jong, J., Tison, J.-L., Chou, L., 2007. Distribution and biogeochemical behaviour of iron in the East Antarctic sea ice. Mar. Chem. 106 (1-2), 18–32. http://dx.doi.org/10.1016/j.marchem.2006.06.010.

Lannuzel, D., Schoemann, V., de Jong, J., Chou, L., Delille, B., Becquevort, S., Tison, J.-L., 2008. Iron study during a time series in the western Weddell pack ice. Mar. Chem. 108 (1-2), 85–95. http://dx.doi.org/10.1016/j.marchem.2007.10.006.

Lannuzel, D., Schoemann, V., de Jong, J., Pasquer, B., van der Merwe, P.,, Masson, F., Bowie, A., 2010. Distribution of dissolved iron in Antarctic sea ice: Spatial, seasonal, and inter-annual variability. J. Geophys. Res. 115 (G3), G03022. http://dx.doi.org/10.1029/2009JG001031.

Lannuzel, D., Bowie, A.R., Remenyi, T., Lam, P., Townsend, A., Ibisanmi, E., Schoemann, V., 2011. Distributions of dissolved and particulate iron in the sub-Antarctic and Polar Frontal Southern Ocean (Australian sector). Deep Sea Res. Part II 58 (21-22), 2094–2112. http://dx.doi.org/10.1016/j.dsr2.2011.05.027.

Lannuzel, D., Merwe, P.C., Van Der, Townsend, A.T., Bowie, A.R., 2014. Size fractionation of iron, manganese and aluminium in Antarctic fast ice reveals a lithogenic origin and low iron solubility. Mar. Chem. 161, 47–56.

Lannuzel, D., Grotti, M., Abelmoshi, M.-L., van der Merwe, P.C. Organic ligands control the concentrations of dissolved iron in Antarctic sea ice. Mar. Chem., Under review.

Martin, J.H., Fitzwater, S.E., 1988. Iron deficiency limits phytoplankton growth in the north-east Pacific subarctic. Nature 331 (6154), 341–343.

Meiners, K.M., Norman, L., Granskog, M.A., Krell, A., Heil, P., Thomas, D.N., 2011. Physico-ecobiogeochemistry of East Antarctic pack ice during the winter-spring transition. Deep Sea Res. Part II 58 (9-10), 1172–1181. http://dx.doi.org/10.1016/j.dsr2.2010.10.033.

Meiners, K.M., Vancoppenolle, M., Thanassekos, S., Dieckmann, G.S., Thomas, D.N., Tison, J.-L., Raymond, B., 2012. Chlorophyll *a* in Antarctic sea ice from historical ice core data. Geophys. Res. Lett. *39* (21), http://dx.doi.org/10.1029/2012GL053478 (n/a–n/a).

Millero, F.J., 1996. Chemical Oceanography, second ed. CRC Press, Boca Raton, FL.

Nicol, S., Pauly, T., Bindoff, N.L., Wright, S., Thiele, D., Hosie, G.W., Woehler, E., 2000. Ocean circulation off east Antarctica affects ecosystem structure and sea-ice extent. Nature 406 (6795), 504–507. http://dx.doi.org/10.1038/35020053.

Palmisano, A.C., Garrison, D.L., 1993. Microorganisms in Antarctic sea-ice, Antarctic Microbiology. I. Friedman. Wiley-Liss, New York, pp. 167–218.

Pollard, R.T., Salter, I., Sanders, R.J., Lucas, M.I., Moore, C.M., Mills, R.A., Zubkov, M.V., 2009. Southern Ocean deep-water carbon export enhanced by natural iron fertilization. Nature 457 (7229), 577–580. http://dx.doi.org/10.1038/nature07716.

Raiswell, R., Benning, L.G., Tranter, M., Tulaczyk, S., 2008. Bioavailable iron in the Southern Ocean: the significance of the iceberg conveyor belt. Geochem. Trans. 9, 1–9. http://dx.doi.org/10.1186/1467-4866-9-7.

Redfield, A.C., 1958. The biological control of chemical factors in the environment. Am. Sci. 46 (3), 205–221.

Riedel, A., Michel, C., Gosselin, M., LeBlanc, B., 2008. Winter-spring dynamics in sea ice carbon cycling in the coastal Arctic Ocean. J. Mar. Syst. 74 (3-4), 918–932.

Roukaerts, A., Cavagna, A.J., Fripiat, F., Lannuzel, D., Mainers, K.M., Dehairs, F., 2016. Determination of the regimes of production in the Antarctic sea-ice during SIPEX-2 using N, & C stable isotope in-situ incubation experiments. Deep Sea Res. Part II, 131, 140–149.

Saenz, B.T., Arrigo, K.R., 2012. Simulation of a sea ice ecosystem using a hybrid model for slush layer desalination. J. Geophys. Res. 117 (C5), C05007. http://dx.doi.org/10.1029/2011JC007544.

Sarmiento, J.G., Gruber, N., 2006. Ocean Biogeochemical Dynamics. Princeton University Press, Princeton, Woodstock p. 503.

Sarthou, G., Timmermans, K.R., Blain, S., Tréguer, P., 2005. Growth physiology and fate of diatoms in the ocean: a review. J. Sea Res. 53 (1-2), 25–42. http://dx.doi.org/10.1016/j.seares.2004.01.007.

Schallenberg, C., van der Merwe, P.C., Chever, F., Cullen, J., Lannuzel, D., Bowie, A. 2016. Dissolved iron distribution in the water column beneath the pack ice in the Eastern Antarctic (120 E) during the winter/spring transition. Deep Sea Res. Part II, 131, 96–110.

Sedwick, P.N., Edwards, P.R., Mackey, D.J., Griffiths, F.B., Parslow, J.S., 1997. Iron and manganese in surface waters of the Australian subantarctic region. Deep Sea Res. Part I 44 (7), 1239–1253.

Smith, R.E.H., Gosselin, M., Kudoh, S., Robineau, B., Taguchi, S., 1997. DOC and its relationship to algae in bottom ice communities. J. Mar. Syst. 11, 71–80.

Sturm, M., R.A. Massom, 2010. Snow and sea ice. In: D. Thomas, G. Dieckman (Eds.), Sea Ice. second ed., Wiley-Blackwell, New York (USA) and Oxford (UK), 153-204.

Tagliabue, A., Sallée, J.-B., Bowie, A.R., Lévy, M., Swart, S., Boyd, P.W., 2014. Surface-water iron supplies in the Southern Ocean sustained by deep winter mixing. Nat. Geosci. 7 (4), 314–320. http://dx.doi.org/10.1038/ngeo21.

Taylor, S.R., 1964. Abundance of chemical elements in the continental crust: a new table. Geochim. Cosmochim. Acta 28, 1273–1285.

Thomas, D.N., Dieckmann, G.S., 2003. Sea Ice—An Introduction to its Physics, Chemistry, Biology and Geology. Blackwell Publishing, Oxford.

van der Merwe, P., Lannuzel, D., Mancuso Nichols, C.A., Meiners, K.M., Heil, P., Norman, L., Bowie, A.R., 2009. Biogeochemical observations during the winter–spring transition in East Antarctic sea ice: evidence of iron and exopolysaccharide controls. Mar. Chem. 115 (3-4), 163–175. http://dx.doi.org/10.1016/j.marchem.2009.08.001.

van der Merwe, P., Lannuzel, D., Bowie, A.R., Mancuso Nichols, C.A., Meiners, K.M., 2011a. Iron fractionation in pack and fast ice in East Antarctica: temporal decoupling between the release of dissolved and particulate iron during spring melt. Deep Sea Res. Part II 58, 1222–1236.

van der Merwe, P., Lannuzel, D., Bowie, A.R., Meiners, K.M., 2011b. High temporal resolution observations of spring fast ice melt and seawater iron enrichment in East Antarctica. J. Geophys. Res. 116 (G3), G03017. http://dx.doi.org/10.1029/2010JG001628.

Weissenberger, J., Grossmann, S., 1998. Experimental formation of sea ice: importance of water circulation and wave action for incorporation of phytoplankton and bacteria. Polar Biol. 20, 178–188.

Worby, A.P., Massom, R.A., Allison, I., Lytle, V.I., Heil, P., 1998. East Antarctic sea ice: A review of its structure, properties and drift, In: (Ed.) Jeffries, M.O., Antarctic Sea Ice: Physical Processes, Interactions and Variability, Antarct. Res. Ser., vol. 74, , AGU, Washington, DC, pp. 41–67.